PROCEEDINGS A

royalsocietypublishing.org/journal/rspa

Research

Cite this article: Wu J, Miller TE, Cicirello A, Taylor G, Mortimer B. 2026 A bio-inspired configuration and algorithm for vibration source localization and its biological implications. *Proc. R. Soc. A* **482**: 20250678. https://doi.org/10.1098/rspa.2025.0678

Received: 3 August 2025
Accepted: 13 January 2026

Subject Areas:
mechanical engineering, biomechanics

Keywords:
vibration source localization, bio-inspired configuration, localization algorithm, spiders

Author for correspondence:
Jun Wu
e-mail: jun.wu@biology.ox.ac.uk

Electronic supplementary material is available online at https://doi.org/10.6084/m9.figshare.c.8297065.

THE ROYAL SOCIETY PUBLISHING

A bio-inspired configuration and algorithm for vibration source localization and its biological implications

Jun Wu[1], Thomas E. Miller[1], Alice Cicirello[2], Graham Taylor[1] and Beth Mortimer[1]

[1]Department of Biology, University of Oxford, Oxford, UK
[2]Department of Engineering, University of Cambridge, Cambridge, UK

JW, 0000-0003-4817-6454; TEM, 0000-0002-9647-570X; GT, 0000-0001-8289-755X; BM, 0000-0002-7230-3647

Vibration source localization is an interdisciplinary topic with applications in both engineering and biology. To inspire technologies for use in engineering and understand how spiders may localize a vibration source, we develop a bio-inspired vibration source localization configuration and algorithm. The algorithm first calculates leg inputs using a backward filter forward smoother algorithm with leg responses; it then estimates the source angle, source distance, substrate wave speed and decay rate through optimization, utilizing the time and amplitude relationships between the calculated leg inputs. The algorithm effectiveness is validated through simulations. Results show that the algorithm gives accurate estimation of the source angle and wave speed with varying source distance, source angle, wave speed and decay rate, with errors typically within 3 deg (absolute) and 6% (relative), respectively. The algorithm cannot estimate the source distance. To locate the position, two spider-like agents would be used collaboratively. The algorithm works well even for leg responses with low signal-to-noise ratio. Results also show that the four-leg combination which includes front and back two legs is the minimum leg

requirement. Increasing the leg–substrate contact damping can improve the algorithm accuracy. These results also give us new insights into how spiders may localize a vibration source.

1. Introduction

Vibration source localization has emerged as an interdisciplinary research topic that has applications in both engineering and biology. In engineering, it is used as a technology to assist in seismic studies and earthquake monitoring [1], to identify impact in equipment to avoid potential failures [2,3] and for indoor vibration event localization [4,5], etc. In biology, many different types of animals are good at vibration source localization, which enables them to detect prey, find mates and avoid predators effectively [6,7], but spiders are arguably the vibration source localization experts [8–10]. By exploring how animals localize the vibration sources, bio-inspired vibration source localization configurations and algorithms can be developed for technological applications. Simultaneously, the application of the algorithms helps us better understand the biological localization behaviour of the animals that inspire it.

In engineering, one application of vibration source localization is the impact identification on beams and plates, which can be classified into two categories: a model-based approach [2,11,12] and a neural network approach [13,14]. The model-based approach requires an accurate dynamic model of the system (i.e. the beam or plate), so the effectiveness is dependent on the ability of the dynamic model to accurately represent the physical system. The advantage is that it only needs the data in one measurement in the operating condition, which is much less than the neural network approach that needs a large number of measurements in different operating conditions. The neural network approach relies on large and diverse datasets for effective training. It is a 'black-box' model that constructs a relationship between the responses and the impact location, while the impact time history usually cannot be calculated. The first step of the model-based approach is to inversely calculate the time history of the input using the structural responses, which can be solved using the dynamic programming method [15–17] or as a two-point boundary-value problem [2,11,12]. The second step involves using an optimization algorithm to estimate the source location [2,11,12]. In most of the engineering applications, the purpose is to identify the impact location or calculate the impact time history [18,19], which only involves one input and is different from the configuration to be proposed, where multiple inputs are transmitted from the vibration source to the spider's eight legs via their spatially distributed points of contact with the substrate.

Another popular engineering application of vibration source localization is the vibration event localization in non-dispersive or dispersive substrates [4,5]. The configuration for vibration source localization is to fix several spatially separated sensors on the substrate. It is usually seen as a travelling wave problem in which the substrate properties are unknown. Localization methods used in engineering can be generally categorized into time difference of arrival (TDOA) method [20], direction of arrival (DOA) method [1], region localization method [4], energy decay method [21], time-reversal method [22], etc. The TDOA method uses the time difference of arrival between different sensors with the assumption of constant wave speed, so it is well-suited for localization in non-dispersive substrates. The DOA method relies on sensors to measure in-plane waves to estimate the source location, which is not applicable when an in-plane wave is not available [1]. The region localization method determines in which region the vibration source is located by partitioning the area into several disjointed regions by the sensors. It is more suitable for the dispersive substrates and the case where the sensors encompass a large area [4]. The energy decay method is based on the fact that the energy decays exponentially with the travelled distance as the wave travels away from the source [21]. Its principle is fundamentally similar to the use of amplitude difference but the use of energy decay makes it also applicable to dispersive substrates. The time-reversal method is based on the principle of time symmetry of wave propagation, and its

Nomenclature	
$\Upsilon_{ij}^{t}/\Upsilon_{ij}$	theoretical/real amplitude ratio between the leg input *i* and input *j*
F_s	sampling frequency
s_i	response of leg *i* or sensor measurement at leg *i*
N_o/N_p	number of outputs/inputs
N	number of generalized coordinates
N_d	number of data sequences
Δt	sampling time interval
R/α	distance/angle of the vibration source from the centre of mass of the spider model/prototype
$\Re_{ij}$	cross-correction between leg input *i* and leg input *j*
u_i	input of leg *i*
V	wave speed
β	decay rate of the substrate
$\Delta t_{ij}^{t}/\Delta t_{ij}$	theoretical/real time difference between the leg input *i* and input *j*

effectiveness depends critically on two conditions: (i) low vibration attenuation in the substrate; (ii) knowledge of wave propagation characteristics. In practical applications where substrates exhibit significant vibration decay and wave speeds are unknown, as in the case examined in this study, the method may suffer from substantially reduced localization accuracy due to signal distortion and impaired time-reversal focusing. In this paper, based on the assumption of non-dispersive substrates, the use of time and amplitude difference is most straightforward and suitable.

In the biological context, there are highly sensitive vibration receptors on spider legs, including slit sensilla and lyriform organs, which enable them to sense vibrational stimuli with amplitudes down to tens of nanometres [23,24]. Spiders use vibration receptors in their legs to enable them to successfully locate a vibration source, enabling them to capture prey and find a mate [8,25]. Spiders localize the vibration source through comparison of vibrational inputs from lyriform organs on all eight legs [8,26]. Across different spider species, it was found that both the amplitude and time differences between leg vibrational inputs have a considerable influence on their orientation to vibration sources [8,25], so do southern green stink bug [27] and deathwatch beetle [28]. Amplitude differences arise due to signal attenuation through the substrates, which varies with material properties and is dependent on the decay rate through the substrate [6,29,30]. Meanwhile, time differences depend on the propagation speed of vibration waves, which can differ significantly between substrates [6,31]. Spiders' strategy for orientation can depend on the substrate's properties and spider ecology [7,31]. If micro-second scale time differences are used as a cue for orientation or vibration source localization, then the fidelity of the spider's sensing system must be very high [25]. Due to the small body dimension and fast wave speeds through silk fibres, it is difficult to extract directional cues from the arrival time difference in the substrate-borne vibrations [28,32]. It is indicated that the legs may be stretched to increase the distance between the legs and the resulting time difference [31].

There are obvious similarities between the vibration source localization problems in biology and engineering. Therefore, by leveraging engineering methodologies and technologies, researchers can enhance the understanding of biological systems and potentially derive inspiration for innovative engineering solutions. Likewise, insights gained from biological processes may contribute to the development of more sophisticated and biologically inspired vibration source localization algorithms or prototype for engineering applications. The biological context of substrate-borne vibration sensing is interesting since animals have evolved optimized structural and sensory mechanisms to utilize vibration sensing for biological functions, even

under variable substrate properties and noisy environmental conditions [7]. This phenomenon is broadly observed in natural systems that exhibit optimized vibration attenuation and sensing mechanism as a result of biological evolution [33]. The limits of biological systems also provide interesting insights for bio-inspired engineering. For spiders, high noise has negative influences on vibration sensing outcomes [34] and spiders can use vibration sensing despite body damage, including sensor ablation [35] or loss of legs [36,37], albeit with functional differences from intact spiders. For similar purposes, researchers have developed computational models of orb webs to investigate what vibrational information the spiders can obtain from the web for vibration source localization in [38–40]. These studies aim to provide insights into the development of novel sensing technologies based on spider web-like structures. Following this direction, researchers have created spider web-inspired tactile sensors capable of localization [41], pressure-strain detection [42], etc. Nevertheless, the development of spider-like prototypes and associated algorithms for vibration source localization has received less research interest. This gap presents an opportunity to create movable devices capable of real-time vibration source localization and tracking, which would represent a significant advancement in the field.

To this end, the primary motivation of this study is to develop bio-inspired configuration and algorithm that can be applied in engineering for vibration source localization. Along the way, our mathematical approach also provides insights into how spiders may localize the vibration source. A bio-inspired vibration source localization configuration is proposed and an associated algorithm is developed in §2. The effectiveness of the algorithm is validated in §3. A discussion is provided in §4, and some conclusions are drawn in §5.

2. Methods

This section is to address the motivation of developing a configuration and algorithm for vibration source localization in this study. Firstly, the bio-inspired vibration source localization configuration is introduced in §2a, and the development of an associated algorithm for vibration source localization is introduced in §2b. Finally, a summary of the localization algorithm is provided in §2c.

(a) Configuration introduction

The bio-inspired configuration has a spider-like structure, which has a body and eight legs connecting to the body, as shown in figure 1. The configuration is mainly based on functional considerations rather than exact biological correspondence. There is at most one sensor embedded in each leg for vibration sensing. The sensors are usually placed at the positions that exhibit nearly maximum vibration responses to leg inputs, ensuring maximum sensitivity and signal-to-noise ratio for vibration sensing. For convenience, the signal that the sensors acquire is assumed to be velocity in this paper, noting that the sensors which are responsible for detecting vibrations in spiders directly transduce cuticular strain. All eight legs rest on the vibrating substrate during vibration source localization. The substrate is assumed to be an idealized unbounded and continuous medium supporting non-dispersive out-of-plane travelling wave. This generalized substrate is used to represent a broad class of engineering structures. The substrate and the spider-inspired prototype are assumed to be dynamically independent. The out-of-plane displacement of the substrate at the distance of L from the vibration source is $\exp(-\beta L)f(t-L/V)$, where β is the decay rate, V is the wave speed, $f(t)$ is the vibration source function with time. The decay rate is used to characterize the spatial attenuation of wave amplitude during propagation through the substrate, accounting for the combined effects of material damping, energy dissipation, etc.

(b) Algorithm development

The associated vibration source localization algorithm is introduced in this section. As shown in figure 2, the first step is to use a backward filter forward smoother algorithm with the known leg

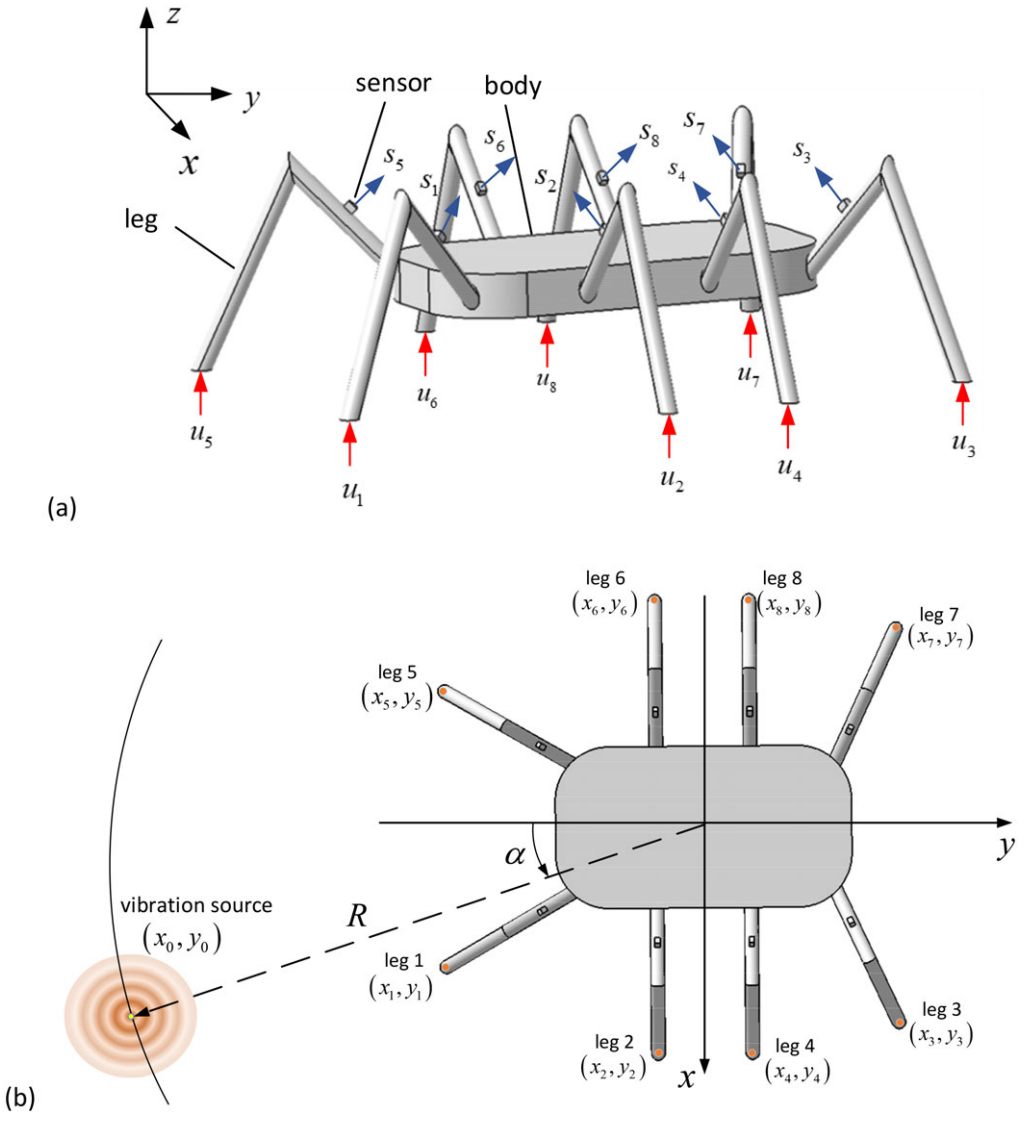

Figure 1. The bio-inspired configuration proposed for vibration source localization: (a) schematic diagram; $u_1, u_2, \ldots, u_8$ represent the leg inputs, while $s_1, s_2, \ldots, s_8$ denote the sensor measurements or leg responses. (b) Top view.

responses to inversely calculate the inputs of the legs. Then in the second step, an optimization which uses the time difference and amplitude difference between different leg inputs and the leg–substrate contact locations is carried out to estimate the vibration source distance, angle, wave speed and decay rate. The detailed theory and method are introduced in the following subsections.

(i) Calculation of inputs (first step)

In this step, it is assumed that the velocity responses of all the considered legs to the excitation of vibration source are known. These responses are derived from the time-domain simulation of a dynamic model in this paper, which, however, will be replaced by experimental response data in real applications. This subsection introduces how to use the leg responses to inversely calculate the leg inputs based on a spider dynamic model. Firstly, the dynamic model and its discrete-time

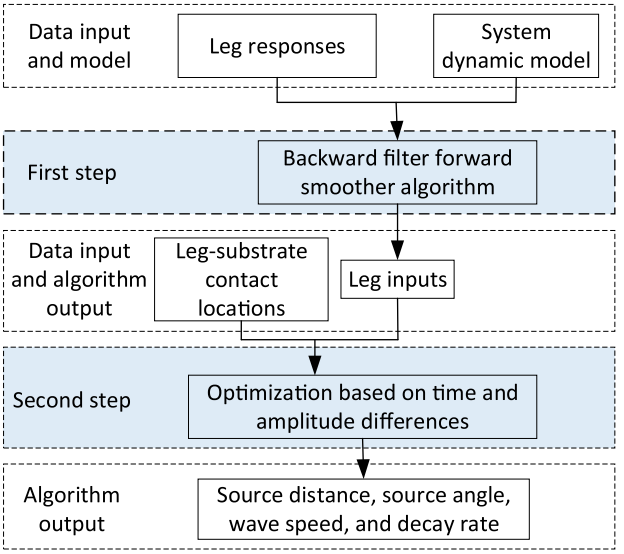

Figure 2. The vibration source localization algorithm.

format are introduced; then, a backward filter forward smoother algorithm is derived to calculate the leg inputs.

Introduction to the dynamic model. The lumped parameter spider dynamic model from a previous study [43] is used. The model has 11 degrees-of-freedom, i.e. bounce of the eight legs and the bounce, pitch and roll of the spider body. It is calibrated against a vibrometry experiment from a real spider (*Grammostola pulchra*) in terms of natural frequencies, damping ratios, mode shapes and vibration transmission in the frequency range of 20–200 Hz. Within the model, it is assumed that there is only one point vibration source, which is defined by the distance from the centre of mass (the origin) of the spider model (R) and an angle α with respect to the $-y$ axis (positive if anti-clockwise) (figure 1). It is also assumed that the vibration source is sufficiently distant from the spider model so that it is not within the region of the spider model's leg span. Furthermore, the vibration in the substrate is assumed to be out-of-plane and exhibit travelling wave behaviour. The vibration from the source transmitting through the substrate is non-dispersive, which means that the wave speed V is constant, independent of the frequency. The vibration from the source decays with a constant decay rate of β when it transmits through the substrate.

To solve the problem numerically, the continuous time equations are converted into discrete time. The state space equations in discrete time are given by (refer to electronic supplementary material S1 for details)

$$\mathbf{z}(n+1) = \boldsymbol{\Phi}\mathbf{z}(n) + \boldsymbol{\Gamma}\mathbf{u}(n) \tag{2.1}$$

and

$$\mathbf{s}(n) = \mathbf{D}_1\mathbf{z}(n) + \mathbf{D}_2\mathbf{u}(n) \tag{2.2}$$

where $\mathbf{z} \in \mathbb{R}^{2N\times 1}$ is the state variable vector, $\mathbf{u} \in \mathbb{R}^{N_p\times 1}$ is the leg displacement input vector, $\mathbf{s} \in \mathbb{R}^{N_o\times 1}$ is the leg response output vector, while $\boldsymbol{\Phi} \in \mathbb{R}^{2N\times 2N}$, $\boldsymbol{\Gamma} \in \mathbb{R}^{2N\times N_p}$, $\mathbf{D}_1 \in \mathbb{R}^{N_o\times 2N}$ and $\mathbf{D}_2 \in \mathbb{R}^{N_o\times N_p}$ are coefficient matrices. The state variable vector $\mathbf{z}$ contains all the state variables used to express the model dynamics. In the spider model, it is related to each leg bounce and body bounce, pitch and roll as well as their time derivatives. The leg displacement input vector $\mathbf{u}$ refers to a vector consisting of the leg inputs, i.e. $u_1, u_2, \ldots, u_8$ in figure 1. The leg response output vector $\mathbf{s}$ refers to a vector consisting of the sensor measurements, i.e. $s_1, s_2, \ldots, s_8$ in figure 1.

Equations (2.1) and (2.2) give the generic form of the dynamic model, i.e. general representation of any possible form of the same model type. The following development of the localization algorithm is based on the generic form, so the localization algorithm is applicable to

any model of the prototype in real applications as long as its dynamics is given in the generic form. The choice of velocity output merely represents one convenient and representative form of the model output. For other outputs, e.g. displacement and acceleration, the dynamic model usually can also be expressed in this generic form, so the following algorithm can be used directly without any further derivations.

Assume the velocity responses of all the considered legs are known, and they are $\mathbf{s}_e(n) \in \mathbb{R}^{N_o \times 1}$. In real measurement using sensors, noise is prone to be introduced in the leg responses. The signal-to-noise ratio (SNR) is defined as the ratio of the mean square of the signal to the mean square of the noise as follows:

$$\mathrm{SNR} = 20\log_{10}\left(\frac{E(\mathrm{signal}^2)}{E(\mathrm{noise}^2)}\right)\ \mathrm{dB}, \tag{2.3}$$

where $E()$ represents the mean value.

If noise is considered, the leg responses $\mathbf{s}_e(n)$ are the summation of the real responses and the noise.

Backward filter forward smoother algorithm. Since there are time and amplitude relationships only between the leg inputs rather than leg responses, the objective of this section is to develop an algorithm that can inversely calculate leg inputs using the known leg responses, then the relationships between the leg inputs can be used to derive the information of the vibration source. To this end, a backward filter forward smoother algorithm is derived through dynamic programming. The derivation can be found in electronic supplementary material S3. The backward filter algorithm runs as follows:

$$\mathbf{Y}_{n-1} = -2\mathbf{E}_n\mathbf{Q}_n^{-1}\mathbf{E}_n^{\mathrm{T}} + \mathbf{D}_1^{\mathrm{T}}\mathbf{W}_s\mathbf{D}_1 + \boldsymbol{\Phi}^{\mathrm{T}}\mathbf{Y}_n\boldsymbol{\Phi} \tag{2.4}$$

and

$$\mathbf{T}_{n-1} = 2\mathbf{E}_n\mathbf{Q}_n^{-1}\mathbf{F}_n - 2\mathbf{D}_1^{\mathrm{T}}\mathbf{W}_s\mathbf{s}_e(n-1) + \boldsymbol{\Phi}^{\mathrm{T}}\mathbf{T}_n, \tag{2.5}$$

where $\mathbf{E}_n = \mathbf{D}_1^{\mathrm{T}}\mathbf{W}_s\mathbf{D}_2 + \boldsymbol{\Phi}^{\mathrm{T}}\mathbf{Y}_n\boldsymbol{\Gamma} \in \mathbb{R}^{2N\times N_p}$ and $\mathbf{F}_n = 2\mathbf{D}_2^{\mathrm{T}}\mathbf{W}_s\mathbf{s}_e(n-1) - \boldsymbol{\Gamma}^{\mathrm{T}}\mathbf{T}_n \in \mathbb{R}^{N_p\times 1}$. $\mathbf{Q}_n = 2\mathbf{D}_2^{\mathrm{T}}\mathbf{W}_s\mathbf{D}_2 + 2\mathbf{W}_u + 2\boldsymbol{\Gamma}^{\mathrm{T}}\mathbf{Y}_n\boldsymbol{\Gamma} \in \mathbb{R}^{N_p\times N_p}$ is a symmetric matrix. $\mathbf{W}_s \in \mathbb{R}^{N_o\times N_o}$ and $\mathbf{W}_u \in \mathbb{R}^{N_p\times N_p}$ are diagonal weighting matrices.

The backward filter algorithm starts from the following initial condition:

$$\mathbf{Y}_{N_d} = \mathbf{D}_1^{\mathrm{T}}(\mathbf{W}_s - \mathbf{W}_s{}^{\mathrm{T}}\mathbf{D}_2\mathbf{P}^{-1}\mathbf{D}_2^{\mathrm{T}}\mathbf{W}_s)\mathbf{D}_1 \tag{2.6}$$

and

$$\mathbf{T}_{N_d} = -2\mathbf{D}_1^{\mathrm{T}}(\mathbf{W}_s - \mathbf{W}_s{}^{\mathrm{T}}\mathbf{D}_2\mathbf{P}^{-1}\mathbf{D}_2^{\mathrm{T}}\mathbf{W}_s)\mathbf{s}_e(N_d), \tag{2.7}$$

where $\mathbf{P} = \mathbf{D}_2^{\mathrm{T}}\mathbf{W}_s\mathbf{D}_2 + \mathbf{W}_u \in \mathbb{R}^{N_p\times N_p}$ is a symmetric matrix.

Then, the forward smoother algorithm runs, and the optimal inputs $\mathbf{u}$, state variables $\mathbf{z}$ and outputs $\mathbf{s}$ are updated as follows:

$$\mathbf{u}(n) = -2\mathbf{Q}_{n+1}^{-1}\mathbf{E}_{n+1}^{\mathrm{T}}\mathbf{z}(n) + \mathbf{Q}_{n+1}^{-1}\mathbf{F}_{n+1}, \tag{2.8}$$

$$\mathbf{z}(n+1) = \boldsymbol{\Phi}\mathbf{z}(n) + \boldsymbol{\Gamma}\mathbf{u}(n), \tag{2.9}$$

and

$$\mathbf{s}(n) = \mathbf{D}_1\mathbf{z}(n) + \mathbf{D}_2\mathbf{u}(n). \tag{2.10}$$

The forward smoother algorithm starts from the known initial condition of $\mathbf{z}(1) = \mathbf{z}_0$. Thus, the optimal inputs $\mathbf{u}$ and model outputs $\mathbf{s}$ can be calculated using the backward filter forward smoother algorithm.

(ii) Parameter estimation using time difference and amplitude difference (second step)

Using the backward filter forward smoother algorithm, the model input vector is calculated. In this step, the leg inputs and the leg-substrate contact locations (x_i, y_i) $(i = 1, 2, \ldots, 8)$ in figure 1 are

used. Theoretically speaking, with the assumptions made in §2a, the input vector should satisfy the following relationship:

$$\begin{cases} \mathbf{u} = \begin{bmatrix} u_1 & u_2 & u_3 & u_4 & u_5 & u_6 & u_7 & u_8 \end{bmatrix}^{\mathrm{T}} \\ \text{and} \quad u_i = \exp(-L_i\beta) f\left(t - \frac{L_i}{V}\right), \end{cases} \tag{2.11}$$

where β is the unknown decay rate, V is the unknown wave speed, $f(t)$ is the unknown vibration source function with time, $L_i = \sqrt{(x_i - x_0)^2 + (y_i - y_0)^2}$ is the distance of the leg–substrate contact location of leg i from the vibration source, (x_i, y_i) is the known coordinate of the leg–substrate contact point of leg i (shown in figure 1), (x_0, y_0) is the unknown coordinate of the vibration source (shown in figure 1), which can also be expressed using the vibration source angle and the distance as

$$\begin{cases} x_0 = R\sin\alpha, \\ y_0 = -R\cos\alpha, \end{cases} \tag{2.12}$$

where R is the vibration source distance, defined from the centre of mass of the spider model (origin) and α is the vibration source angle (shown in figure 1).

Once the inputs are calculated, the relationships between the leg inputs can be used to estimate the wave speed V, decay rate β, vibration source angle α and distance R. The following subsections show how to use the time and amplitude differences to estimate these parameters.

Time difference. There is a time difference between different inputs, because the vibration takes a different time to travel from the vibration source to different legs. The real time difference can be calculated first by calculating the cross-correlation $\Re_{ij}$ between two leg inputs u_i and u_j, which is defined as

$$\Re_{ij}(m) = \begin{cases} \sum_{n=1}^{N_d - m} u_i(n+m)u_j(n), m \geq 0, \\ \Re_{ji}(-m), m < 0. \end{cases} \tag{2.13}$$

Then, the real time difference is calculated by finding m for which the cross-correlation $\Re_{ij}(m)$ reaches the maximum, and then dividing it by the sampling frequency F_s as follows:

$$\Delta t_{ij} = \arg\max_m \Re_{ij}(m)/F_s, \tag{2.14}$$

where Δt_{ij} is the real time difference between u_i and u_j.

According to the relationships between the inputs in equation (2.11), the theoretical time difference is given by

$$\Delta t_{ij}{}^t(\alpha, R, V) = \Delta L_{ij}/V, \tag{2.15}$$

where $\Delta L_{ij} = L_i - L_j$ is the distance difference from the leg–substrate contact locations of leg i and leg j to the vibration source.

The theoretical time difference should be a function of the wave speed V, source distance R and source angle α. To estimate the wave speed V, source distance R and source angle α using the time difference, the real time difference calculated by cross-correlation can be used as the target and the parameters are optimized to make the theoretical time difference approach it as much as possible, so the objective function is given by

$$\mathrm{obj}_1 = \sum_{i \in \mathbf{G}} \sum_{j > i, j \in \mathbf{G}} |\Delta t_{ij}{}^t(\alpha, R, V) - \Delta t_{ij}|, \tag{2.16}$$

where $\mathbf{G}$ represents the set of leg sequence numbers whose responses are considered.

Through optimization, the wave speed V, source distance R and source angle α can be estimated.

The distance difference ΔL_{ij} is given by

$$\begin{aligned}\Delta L_{ij} &= \sqrt{(x_0 - x_i)^2 + (y_0 - y_i)^2} - \sqrt{(x_0 - x_j)^2 + (y_0 - y_j)^2} \\ &= \frac{(x_i^2 + y_i^2) - (x_j^2 + y_j^2) - 2R(x_i - x_j)\sin\alpha + 2R(y_i - y_j)\cos\alpha}{\sqrt{R^2 + x_i^2 + y_i^2 - 2Rx_i\sin\alpha + 2Ry_i\cos\alpha} + \sqrt{R^2 + x_j^2 + y_j^2 - 2Rx_j\sin\alpha + 2Ry_j\cos\alpha}}. \quad (2.17)\end{aligned}$$

It can be found that ΔL_{ij} converges when the source distance R becomes very large, as follows:

$$\lim_{R\to\infty} \Delta L_{ij} = \sin\alpha(x_j - x_i) + \cos\alpha(y_i - y_j). \quad (2.18)$$

This results in the theoretical time difference being independent of the source distance R when the source distance is much larger than the leg span, so that the theoretical time difference is only a function of the source angle α and wave speed V, given as follows:

$$\lim_{R\to\infty} \Delta t_{ij}{}^t(\alpha, R, V) = \Delta t_{ij}{}^t(\alpha, V). \quad (2.19)$$

This indicates that when the source distance R becomes much larger than the leg span, the change in source distance only results in negligible change in the theoretical time difference, so it makes the estimation of source distance very difficult or even impossible. It can also be seen from equation (2.15) that the theoretical time difference is in inverse proportion to the wave speed V, so increasing the wave speed decreases the theoretical time difference between the inputs, which will make the localization using time difference more difficult.

Amplitude difference. Due to the decay of the vibration in the substrate, there is also an amplitude difference between different inputs. The real amplitude ratio between two inputs u_i and u_j can be calculated first by finding the peaks of u_i and then calculating the ratios with the corresponding values of u_j after shifting according to the cross-correlation, and finally calculating the geometric mean of the ratios, given as follows:

$$\Upsilon_{ij} = \left[\prod_{n=1}^{N_e} \frac{u_i(\boldsymbol{\varphi}(n))}{u_j(\boldsymbol{\varphi}(n) - m)}\right]^{1/N_e}, \text{where } \boldsymbol{\varphi} = \arg\operatorname*{peak}_n u_i(n), m = \arg\max_m \Re_{ij}(m), \quad (2.20)$$

where peak $u_i(n)$ means finding the peaks of u_i and $\boldsymbol{\varphi} = \arg\operatorname*{peak}_n u_i(n)$ means the indexes of the peaks of u_i; $\boldsymbol{\varphi}(n)$ means the index of the n^{th} peak of u_i, and $\boldsymbol{\varphi}(n) - m$ stands for the corresponding index of the value in u_j, N_e is the total number of peaks considered.

According to the relationships between the inputs in equation (2.11), the theoretical amplitude ratio is given by

$$\Upsilon_{ij}{}^t(\alpha, \beta, R) = \exp(-\Delta L_{ij}\beta). \quad (2.21)$$

It is a function of the decay rate β, source distance R and source angle α.

To estimate the decay rate β, source distance R and source angle α using the amplitude ratio, the real amplitude ratio calculated in equation (2.20) is used as the target and the parameters are optimized to make the theoretical amplitude ratio approach it as much as possible, so the objective function is given by

$$\text{obj}_2 = \sum_{i\in\mathbf{G}} \sum_{j>i, j\in\mathbf{G}} \left|\ln \Upsilon_{ij}{}^t(\alpha, \beta, R) - \ln \Upsilon_{ij}\right|, \quad (2.22)$$

where $\mathbf{G}$ represents the set of leg sequence numbers whose responses are considered.

Through optimization, the decay rate β, source distance R and source angle α can be estimated.

For the same reason, when the source distance is very large, the theoretical amplitude ratio is only a function of the source angle α and decay rate β, as follows:

$$\lim_{R\to\infty} \Upsilon_{ij}{}^t(\alpha, \beta, R) = \Upsilon_{ij}{}^t(\alpha, \beta). \quad (2.23)$$

Thus, when the source distance is very large, using amplitude difference to estimate the source distance R becomes very difficult or even impossible. It can also be seen from equation (2.21) that

when the decay rate β is close to zero, the theoretical amplitude ratio between inputs becomes close to 1 and is not a function of the source distance R and source angle α any more. This will make the vibration source localization using amplitude difference very difficult.

When both the time difference and amplitude difference are used, then the objective function is given by

$$\text{obj} = w_1 \text{obj}_1 + w_2 \text{obj}_2, \tag{2.24}$$

where w_1 and w_2 are the weighting factors.

(c) Summary of the vibration source localization algorithm

Based on the previous subsections, a bio-inspired vibration source localization configuration is proposed and the associated algorithm is developed and illustrated in figure 2. The process is described as follows:

1. The system dynamic model and leg vibration responses to the vibration source should be available. The dynamic model is derived through mathematical modelling of a real spider in this paper [43] or spider-like prototype in real applications, while the leg responses are derived from the time-domain simulation of the dynamic model in this paper or from real response data in real applications. The localization algorithm can be used directly as long as the model is expressed in the generic state space form in equations (2.1) and (2.2).
2. Running the backward filter forward smoother algorithm (equations (2.4), (2.5), (2.8) and (2.9)) using the system dynamic model and available leg responses to obtain the inputs **u**;
3. With the use of the leg–substrate contact locations, running an optimization algorithm using the time and amplitude differences of the derived inputs, i.e. minimizing the objective function in equation (2.24). The optimization is implemented with a global–local mixed algorithm introduced in [44], with all the optimization variables (i.e. source distance, source angle, wave speed and decay rate) constrained in reasonable ranges.
4. Obtaining source distance, source angle, wave speed and decay rate from the optimization algorithm.

3. Results

To validate the effectiveness of the proposed vibration source localization algorithm, parameter estimation is carried out with varying source distance, source angle, wave speed and decay rate. Fundamentally speaking, the source distance can only be estimated in the given configuration when the source distance is comparable to the spider leg span, since all the parameters can only be estimated by comparing between the leg inputs. Therefore, the effectiveness of the algorithm is evaluated mainly by its accuracy in estimating the source angle, while the estimation of the wave speed and decay rate is not used as an evaluation criterion for the effectiveness of the algorithm.

The procedure of validating the effectiveness of the algorithm is shown in figure 3. Firstly, the leg outputs are derived from the time-domain simulation of the dynamic model with the given leg inputs generated through a substrate model. Then, the localization algorithm uses the leg reponses and leg–ground contact locations as the inputs and outputs the estimated parameters. Finally, the estimated parameters are compared with the real ones to validate the effectiveness of the localization algorithm. In the time-domain simulation of the dynamic model, the vibration source function is assumed to be a sinc function as follows:

$$f(t) = \begin{cases} \frac{0.1\sin(200\pi(t-0.25)/3)}{200(t-0.25)/3}, & 0.1\text{s} \le t \le 0.4\text{ s}, \\ 0, & \text{otherwise.} \end{cases} \tag{3.1}$$

The sinc function has an ideal rectangular spectrum. Therefore, it is chosen to represent a broadband excitation, enabling effective evaluation of the localization algorithm performance. Since one of the advantages of the algorithm is that it is not dependent on the vibration

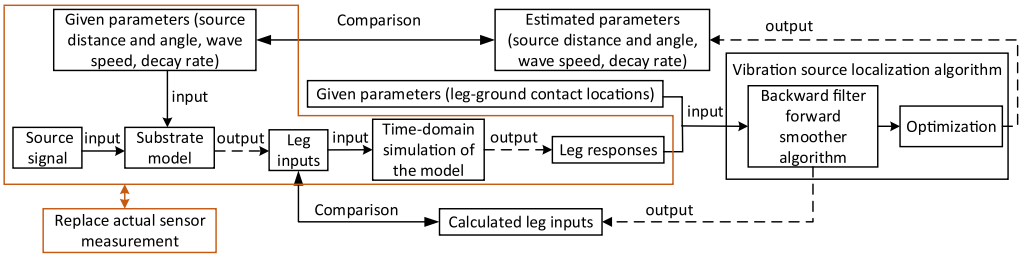

Figure 3. The procedure of algorithm validation.

Table 1. The parameters of the reference operation condition and optimization range.

parameters	value	optimization range
source distance R (m)	3	0.05–100
wave speed V (ms^{-1})	10	0.1–200
source angle α (deg)	60	0–360
decay rate β (m^{-1})	2	0–20

source function, the effectiveness of the algorithm can also be validated using other functions. The dynamic model is simulated in Matlab/Simulink with the given vibration source function equation (3.1) and parameters. All the model parameters are listed in [43]. The velocity responses of the legs in the simulation are used to replace the actual measurement of the sensors $\mathbf{s}_e(n)$. The simulation is carried out using a fixed-step ode4 solver with a step size of 1/30 000 s and a duration of 1.5 s.

The parameters of the reference operation condition are listed in table 1. One of the parameters is changed while the others are kept the same in the following studies. The weighting matrices are $\mathbf{W}_s = \mathbf{I}_{N_o \times N_o}$ and $\mathbf{W}_u = 10^{-3}\mathbf{I}_{N_p \times N_p}$. The matrix $\mathbf{W}_u$ is related to the regularization term, so it is obtained empirically through trial-and-error to balance data-fitting accuracy and input smoothness. All eight leg responses are considered except in §3f where different leg combinations are considered. Noise is added in the leg responses only in §3e–3g. In the reference condition, the results derived from the backward filter forward smoother algorithm are shown in figures 4 and 5. Figure 4 shows the comparison between the calculated velocity outputs and real model velocity outputs for all eight legs, which are $\mathbf{s}(n)$ and $\mathbf{s}_e(n)$, respectively. Since the backward filter forward smoother algorithm aims to minimize their differences, the outputs show good consistency for all eight legs. The calculated inputs and the real model inputs for all eight legs are compared in figure 5, which are $\mathbf{u}$. Generally, the inputs show good agreement, especially in terms of the phase. Figures 4 and 5 show that the backward filter forward smoother algorithm is valid in terms of calculating the real model leg inputs. However, some obvious difference in amplitude can be seen, especially in the peaks. For this reason, the weighting w_1 (chosen to be 50) is much larger than w_2 (chosen to be 1) in the objective function equation (2.24). This choice also makes sense considering that amplitude difference can be affected by noise, drift, error of sensor sensitivity, etc. in real measurements, while modern sensors can distinguish tiny time difference and is less affected by these factors.

(a) Varying source distance

In this subsection, the source distance is changed while other parameters are kept the same as the reference parameters in table 1. The parameter estimations with varying source distance are illustrated in table 2. The estimation of the source distance (R) is only relatively accurate when the distance is less than 0.1 m, about 1.25 times the leg span considering the model has an approximate

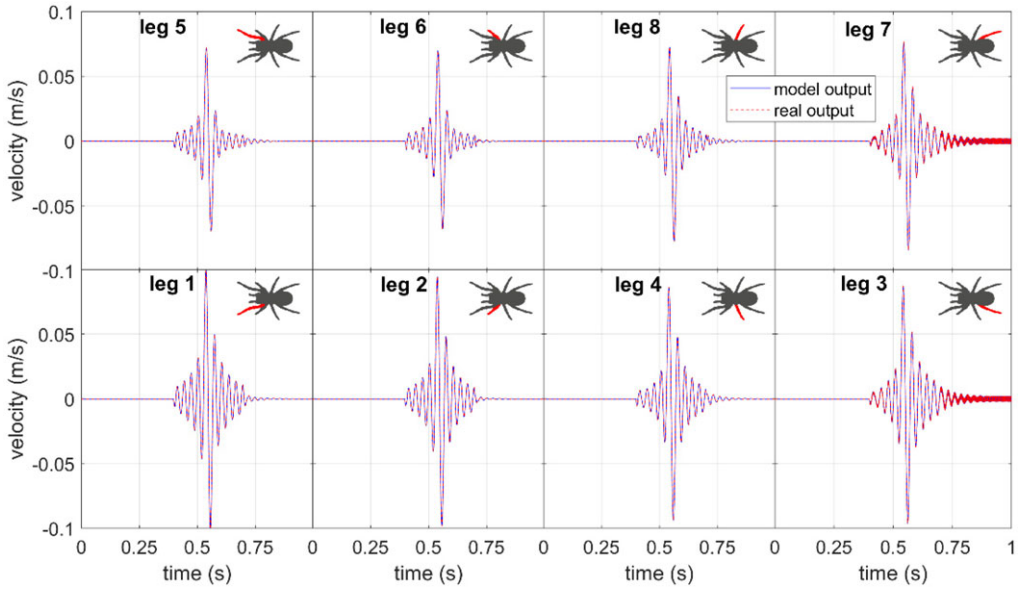

Figure 4. The comparison between the real model outputs (red) and the calculated outputs (blue). The real model outputs are the real model leg velocity responses, while the calculated outputs are the leg velocity responses calculated from the backward filter forward smoother algorithm. The spider icon in each subfigure is only for illustration purpose with the red leg being the leg corresponding to the subfigure.

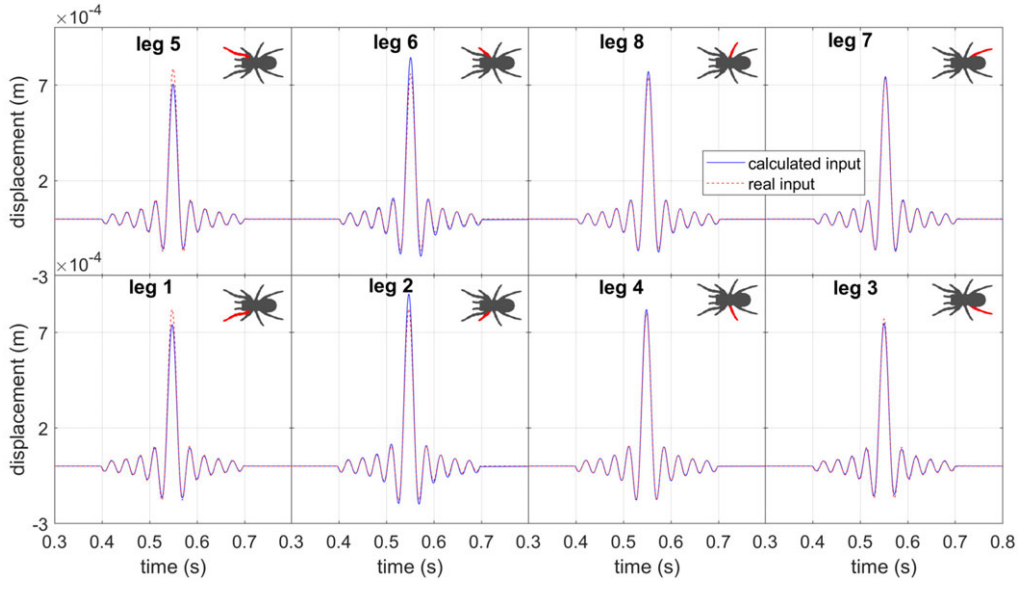

Figure 5. The comparison between the real model inputs (red) and the calculated inputs (blue). The real model inputs are the vibrations transmitted to the leg–substrate contact locations from the vibration source, while the calculated inputs are the vibrations at the leg–substrate contact locations calculated from the backward filter forward smoother algorithm. The spider icon in each subfigure is only for illustration purpose with the red leg being the leg corresponding to the subfigure. '$t = 0$' is the time when the simulation starts.

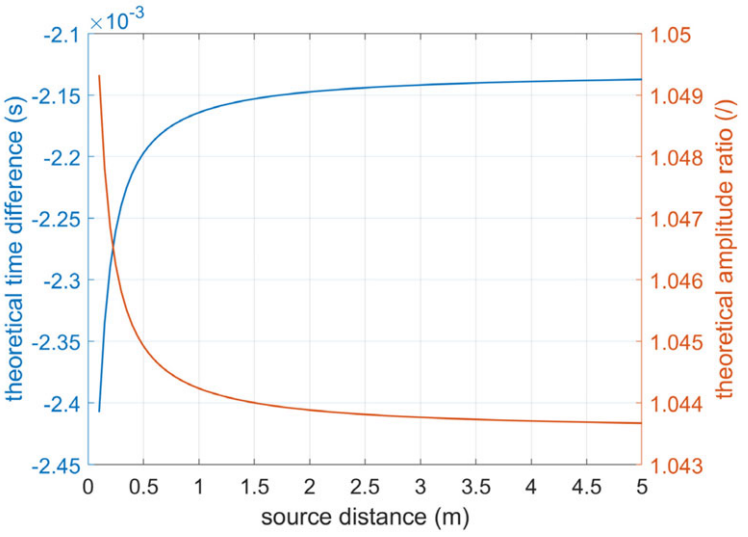

Figure 6. The change of the theoretical time difference and theoretical amplitude ratio between leg 1 and leg 5 with the source distance.

Table 2. Parameter estimation with varying source distance. Errors for source distance, wave speed and decay rate are expressed as relative error, while error for source angle is given as absolute error.

	source distance R		source angle α		wave speed V		decay rate β	
actual source distance (m)	estimate (m)	rel err (%)	estimate (deg)	abs err (deg)	estimate (ms^{-1})	rel err (%)	estimate (m^{-1})	rel err (%)
0.06	0.070	16.7	61.52	1.52	10.35	3.5	1.29	35.5
0.1	0.107	7.0	60.63	0.63	10.59	5.9	1.20	40.0
0.15	0.216	44.0	60.75	0.75	10.12	1.2	1.23	38.5
0.2	0.358	79.0	60.71	0.71	10.20	2.0	1.25	37.5
0.5	90.89	$\gg$100	60.41	0.41	10.17	1.7	1.27	36.5
1	75.63	$\gg$100	59.80	0.20	10.17	1.7	1.28	36.0
3	90.12	$\gg$100	59.77	0.23	10.17	1.7	1.28	36.0
5	95.41	$\gg$100	59.77	0.23	10.17	1.7	1.28	36.0
7	54.25	$\gg$100	59.78	0.23	10.17	1.7	1.28	36.0
9	90.84	$\gg$100	59.77	0.23	10.17	1.7	1.28	36.0
10	89.69	$\gg$100	59.77	0.23	10.18	1.8	1.28	36.0

leg span of 0.08 m. When the distance is larger than 0.1 m, the theoretical time differences and amplitude ratios do not show much difference with the increase of source distance, which makes the estimation of source distance difficult or even impossible. Figure 6 shows the change of the theoretical time difference and theoretical amplitude ratio between leg 1 and leg 5 with the source distance. Both converge and do not show much difference with the increase of source distance. Since the estimation of the source distance R is not good at the reference distance of 3 m, its estimation values are not illustrated in the following subsections. The estimation of the source angle (α) is very accurate with an absolute error less than 2 deg even when the source distance is up to 10 m. The estimation of the wave speed (V) is also accurate with a relative error within

Table 3. Parameter estimation with varying source angles. Errors for wave speed and decay rate are expressed as relative error, while error for source angle is given as absolute error.

	source angle α		wave speed V (ms^{-1})		decay rate β (m^{-1})	
actual angle (deg)	estimate (deg)	abs err (deg)	estimate (ms^{-1})	rel err (%)	estimate (m^{-1})	rel err (%)
0	0	0.0	9.85	1.5	0.93	53.5
10	9.65	0.35	9.84	1.6	1.16	42.0
20	19.31	0.31	9.88	1.2	1.36	32.0
30	29.05	0.95	9.93	0.7	1.40	30.0
40	38.91	1.09	10.05	0.5	1.37	31.5
50	49.25	0.75	10.13	1.3	1.33	33.5
60	59.78	0.22	10.17	1.7	1.28	36.0
70	70.55	0.55	10.17	1.7	1.24	38.0
80	80.62	0.62	10.12	1.2	1.21	39.5
90	90.16	0.16	10.13	1.3	1.16	42.0
100	99.97	0.03	10.13	1.3	1.37	31.5
110	109.82	0.18	10.11	1.1	1.44	28.0
120	120.06	0.06	9.89	1.1	2.33	16.5
130	130.70	0.70	9.97	0.3	2.68	34.0
140	140.34	0.34	9.94	0.6	3.46	73.0
150	150.60	0.60	9.90	1.0	3.28	64.0
160	160.35	0.35	9.78	2.2	3.21	60.5
170	170.51	0.51	9.74	2.6	3.19	59.5
180	180.00	0.0	9.80	2.0	3.23	61.5

6%. The estimation of the decay rate (β) is less accurate with relative error reaching 40%, which is ascribed to the fact that there is amplitude difference between the real inputs and the calculated inputs.

It should be noted that when the source distance becomes large, the vibration transmitted to the spider model becomes small in magnitude, so the leg responses are prone to be influenced by the noise. For example, when the source distance is 10 m, the displacement input magnitude for the legs is in the order of 10^{-10} m. Thus, it can be concluded that the localization algorithm gives an estimation of the source angle accurate to within 2 deg with varying source distance as long as the vibration transmitted to the spider model is large enough in magnitude to be successfully detected above noise.

(b) Varying source angle

In this subsection, the source angle is changed while other parameters are kept the same as the reference parameters in table 1. Due to the symmetry, the source angle is changed from 0 to 180 deg (see the definition of source angle α in figure 1). The parameter estimations with an angle increment of 10 deg are illustrated in table 3. The estimation errors of the source angle (α) and wave speed (V) are within 1.5 deg (absolute) and 3% (relative), respectively. The relative estimation error of the decay rate (β) is relatively large, up to 73%. These results prove that the

Table 4. Parameter estimation with varying wave speed. Errors for wave speed and decay rate are expressed as relative error, while error for source angle is given as absolute error.

	wave speed V		source angle α		decay rate β	
actual wave speed (m/s)	estimate (ms^{-1})	rel err (%)	estimate (deg)	abs err (deg)	estimate (m^{-1})	rel err (%)
5	5.15	3.0	59.77	0.23	0.47	76.5
10	10.17	1.7	59.78	0.22	1.28	36.0
20	20.09	0.5	60.95	0.95	1.52	24.0
30	29.94	0.2	61.53	1.53	1.61	19.5
40	39.67	0.8	62.30	2.30	1.66	17.0
50	49.56	0.9	63.37	3.37	1.84	8.0
60	58.74	2.1	63.21	3.21	1.87	6.5
70	67.87	3.0	63.73	3.73	1.86	7.0
80	77.90	2.6	64.68	4.68	1.82	9.0
90	88.26	1.9	64.75	4.75	1.80	10.0
100	101.09	1.1	64.54	4.54	2.14	7.0

localization algorithm gives an estimation of the source angle accurate to within 2 deg for all source angles.

(c) Varying wave speed

In this subsection, the wave speed is changed while other parameters are kept the same as the reference parameters in table 1. The parameter estimations with varying wave speed are illustrated in table 4. When the wave speed is increased to 100 ms^{-1}, the errors of the source angle estimation (α) and wave speed estimation (V) are always within 5 deg (absolute) and 3% (relative), respectively. The results show that the absolute error of the source angle estimation becomes large with the increasing wave speed. This is because increasing wave speed reduces the time difference, which makes the estimation using time difference more difficult (§2b(i) *Introduction to the dynamic model*). The time difference is in proportion to the size of the spider model according to equation (2.15). Therefore, a larger spider model size leads to a larger time difference, which enables accurate estimation under higher wave speeds. The estimation of the decay rate (β) is still less accurate, especially for low wave speeds. The relative estimation error reaches 76.5% when the wave speed is 5 ms^{-1}, but the error reduces with the increasing wave speed. These results prove that the localization algorithm gives an estimation of the source angle accurate to within 5 deg for a wide range of wave speeds.

(d) Varying decay rate

In this subsection, the decay rate is changed while other parameters are kept the same as the reference parameters in table 1. The parameter estimations with varying decay rate are illustrated in table 5. The absolute error of the source angle (α) estimation is within 1 deg, while the relative error of the wave speed (V) estimation is within 3%. There is relatively high absolute error for the decay rate (β) estimation, and the error reaches 100%. It should be noted that when the decay rate is too large, the vibration transmitted to the spider model becomes very small, so the responses are prone to be influenced by noise. For example, when the decay rate is 9 m^{-1}, the displacement input magnitude for the legs is in the order of 10^{-13} m. Thus, it can be concluded that the localization algorithm gives an estimation of the source angle accurate to within 1 deg

Table 5. Parameter estimation with varying decay rate. Errors for wave speed and decay rate are expressed as relative error, while error for source angle is given as absolute error.

	decay rate β		source angle α		wave speed V	
actual decay rate (m^{-1})	estimate (m^{-1})	rel err (%)	estimate (deg)	abs err (deg)	estimate (ms^{-1})	rel err (%)
0	0	0.0	59.51	0.49	10.23	2.3
0.5	0	100	59.50	0.50	10.23	2.3
1	0.35	65.0	59.45	0.55	10.17	1.7
2	1.28	36.0	59.78	0.22	10.17	1.7
3	2.21	26.3	59.78	0.22	10.17	1.7
4	3.14	21.5	60.05	0.05	10.11	1.1
5	4.11	17.8	60.05	0.05	10.10	1.0
6	5.08	15.3	60.31	0.31	10.11	1.1
7	6.09	13.0	60.24	0.24	10.04	0.4
8	7.07	11.6	60.27	0.27	10.04	0.4
9	8.06	10.4	60.15	0.15	9.97	0.3

with varying decay rate as long as the vibration transmitted to the spider model is large enough in magnitude to be successfully detected above noise.

(e) Influence of noise

The previous calculations are carried out in ideal conditions where there is no noise in the leg responses. However, noise is inevitable in real measurement using sensors. In this subsection, the influence of noise on the effectiveness of the localization algorithm is studied. The noise used is a random noise under a uniform distribution between $-A_p$ and A_p. The mean of the noise is always 0, while the variance of the noise is $A_p^2/3$. The same level of noise is added to the eight leg velocity responses. The noise is randomly generated, so it is different for different legs.

The comparison between the inputs and between the outputs using the backward filter forward smoother algorithm in the case of uniformly distributed noise with a mean of 0 and variance of 3.33×10^{-5} is illustrated in electronic supplementary material, figures S1 and S2 (supplementary material S4). The addition of the noise in leg responses introduces the noise in the calculated inputs, especially for legs 6, 7, 2 and 3 (due to the low leg–substrate contact damping). The parameter estimations with different noise levels are illustrated in table 6. Since the noise is randomly generated, the estimation results are different for each run of the localization algorithm. The ranges, means and standard deviations of the estimated parameters in 10 runs of the localization algorithm are listed. The standard deviations show an increasing tendency with the increasing noise level, which is consistent with the increasing uncertainty with the increasing noise level. The absolute error of the source angle (α) estimation is within 3 deg, while the relative error of the wave speed (V) estimation is within 5%. There is still high absolute error for the decay rate (β) estimation. These results show that the localization algorithm gives an estimation of the source angle accurate to within 3 deg even under high noise level.

(f) Influence of leg number and combination

In previous subsections, all eight leg responses are considered. However, eight legs may not be the minimum number for accurate vibration source localization, raising the possibility that some legs can be neglected while the localization accuracy does not reduce much. To investigate the

Table 6. Parameter estimation with different noise levels. Errors for wave speed and decay rate are expressed as relative error, while error for source angle is given as absolute error.

noise level				source angle α		wave speed V		decay rate β	
			SNR[a]	estimate[b]	abs err[c]	estimate	rel err	estimate	rel err
A_p	mean	variance	(dB)	(deg)	(deg)	(ms^{-1})	(%)	(m^{-1})	(%)
0.002	0	1.33×10^{-6}	39–46	59.76–60.74 (60.38, 0.30)	0.74	9.99–10.24 (10.14, 0.07)	2.4	1.79–2.70 (2.09, 0.30)	35.0
0.004	0	5.33×10^{-6}	27–34	59.87–60.93 (60.52, 0.34)	0.93	9.80–10.37 (10.15, 0.20)	3.7	1.16–3.25 (2.20, 0.73)	62.5
0.006	0	1.2×10^{-5}	19–27	60.01–61.24 (60.61, 0.42)	1.24	9.79–10.32 (10.01, 0.18)	3.2	1.16–3.71 (2.44, 0.74)	85.5
0.008	0	2.13×10^{-5}	14–22	59.45–61.19 (60.51, 0.59)	1.19	10.09–10.35 (10.20, 0.09)	3.5	0.86–5.85 (3.06, 1.64)	$\gg$100
0.010	0	3.33×10^{-5}	11–18	59.40–62.34 (60.73, 0.87)	2.34	9.83–10.42 (10.07, 0.21)	4.2	0.74–5.45 (3.64, 1.40)	$\gg$100

[a]It is the range of SNR for eight leg velocity responses.

[b]The estimation results are the ranges, the means (first parameter in the bracket) and standard deviations (second parameter in the bracket) of the estimated parameters in 10 runs.

[c]The error is the maximum error in 10 runs.

royalsocietypublishing.org/journal/rspa *Proc. R. Soc. A* **482**: 20250678

minimum number of legs needed and the corresponding leg combinations, parameter estimations with different leg combinations are illustrated in electronic supplementary material, table S1 in the electronic supplementary material S5, which is carried out in the case of uniformly distributed noise with a mean of 0 and variance of 1.33×10^{-6}. The ranges, means and standard deviations of the estimated parameters in 10 runs of the algorithm are listed due to the randomly generated noise. Some of the results are also illustrated in table 7. For details, refer to electronic supplementary material S5.

The comparison between different leg combinations shows that for any combinations that include the front (1 and 5) and back two (3 and 7) legs, the localization algorithm can always give accurate estimations of the source angle and wave speed, whose errors are usually within 4 deg (absolute) and 8% (relative), respectively. Increasing the number of legs to this basis can increase the estimation accuracy, but more equipment is needed (e.g. sensors) and the running time of the algorithm will be increased. Therefore, the 1–3–5–7 combination can be seen as the minimum leg requirement. The estimations will not be accurate with absolute error of source angle estimation beyond 4 deg if one or two or three legs are removed from legs 1, 3, 5 or 7.

(g) Influence of leg–substrate contact damping

The model parameters that may influence the effectiveness of the localization algorithm are the leg–substrate contact damping. In order to study its influence, all the leg–substrate contact damping is increased to $0.44\,\mathrm{Nsm}^{-1}$, the same damping as the original damping of legs 1 and 5. electronic supplementary material, figure S3 (in the electronic supplementary material S5) shows the comparison between the real leg inputs and calculated inputs when the leg–substrate contact damping is increased. Compared with electronic supplementary material, figure S2, the noise in the calculated leg inputs is obviously reduced. The parameter estimations with different noise levels after increasing the leg–substrate contact damping are illustrated in table 8. Compared with table 6, increasing the leg–substrate contact damping reduces the noise in the calculated leg inputs, so the estimation accuracy of the source angle, wave speed and decay rate shows obvious improvement.

4. Discussion

(a) Biological relevance and implication

Although the present study is based on simulations rather than biological experiments, the analyses and results in the previous sections give insight into how spiders may localize vibration sources in a naturally occurring context. The discussion below aims to interpret the engineering results in a biological context and to propose testable hypotheses for future biological studies.

As expected, a spider is theoretically able to use either time difference or amplitude difference to determine the direction of the vibration source, as we have shown that source angle can be estimated by either method. In addition, analyses in §2b(ii) show that if the spider uses the time or amplitude difference between the legs for localization, it can also theoretically estimate the wave speed and decay rate. However, it remains unclear whether the spider could derive any practical benefit from estimating wave speed and decay rate beyond orientating to the source.

In the real animal, physiological constraints act to determine whether time or amplitude differences between two vibration inputs at different mechanosensor locations across the body can be detected or distinguished. It is reported that the minimum time difference that spiders (*Cupiennius salei*) can detect is around 2–4 ms [8,45,46]. If the wave speed in the substrate is high, which depends on substrate properties [25,45], it will be difficult for the spiders to localize using time difference, as is proposed for orb weaving spiders on silk webs [25,45]. However, for ground dwelling spiders such as tarantulas, upon which our simulations are based [43], the wave speeds will be lower and thus time differences can be above the physiological threshold, so can be used for orientation. For the same reasons, if the decay rate of the substrate is very small, it will be

Table 7. Parameter estimation with different leg numbers and combinations in the case of uniformly distributed noise with a mean of 0 and variance of 1.33×10^{-6}. Red legs in the spider icon represent the legs considered. Errors for wave speed and decay rate are expressed as relative error, while error for source angle is given as absolute error.

			source angle α		wave speed V		decay rate β	
leg combination			estimate[a] (deg)	abs err[b] (deg)	estimate (ms^{-1})	rel err (%)	estimate (m^{-1})	rel err (%)
eight legs	1–2–3–4–5–6–7–8		59.76–60.74 (60.38, 0.30)	0.74	9.99–10.24 (10.14, 0.07)	2.4	1.79–2.70 (2.09, 0.30)	10.5
four legs	1–3–5–7		63.35–63.67 (63.58, 0.12)	3.67	9.25–9.33 (9.28, 0.02)	7.5	0–1.84 (0.48, 0.63)	100
	2–4–6–8		10.38–15.53 (13.24, 1.81)	49.62	14.01–18.03 (15.96, 1.08)	80.3	8.83–11.56 (9.98, 0.91)	$\gg$100
three legs	1–5–7		100.74–102.37 (101.58, 0.56)	42.37	8.10–8.24 (8.19, 0.04)	19.0	18.25–20 (19.57, 0.68)	$\gg$100
	1–3–7		321.65–323.15 (322.25, 0.53)	263.15	9.24–9.52 (9.34, 0.10)	7.6	13.47–18.47 (16.72, 1.59)	$\gg$100
five legs	1–3–5–7–2		63.03–63.58 (63.46, 0.17)	3.58	9.39–9.64 (9.52, 0.09)	6.1	0–1.88 (0.85, 0.76)	100
	1–3–5–7–6		59.80–61.74 (60.75, 0.60)	1.74	9.59–9.81 (9.72, 0.07)	4.1	0–1.12 (0.42, 0.40)	100
six legs	1–3–5–7–2–6		60.09–61.36 (60.75, 0.39)	1.36	10.18–10.56 (10.48, 0.12)	5.6	0.67–2.73 (1.70, 0.56)	66.5
	1–3–5–7–4–8		62.44–62.97 (62.75, 0.16)	2.97	9.39–9.58 (9.44, 0.06)	6.1	0.37–1.78 (0.88, 0.50)	81.5
seven legs	1–3–5–7–2–6–8		58.87–60.67 (59.90, 0.57)	1.13	10.23–10.33 (10.28, 0.04)	3.3	0.19–2.94 (2.02, 0.80)	90.5
	1–3–5–7–2–4–6		59.92–61.53 (61.06, 0.45)	1.53	9.79–10.54 (10.26, 0.25)	5.4	0.53–1.14 (0.86, 0.22)	73.5

[a]The estimation results are the ranges, the means (first parameter in the bracket) and standard deviations (second parameter in the bracket) of the estimated parameters in 10 runs.
[b]The error is the maximum error in 10 runs.

Table 8. Parameter estimation with different noise levels when all the leg–substrate contact damping is increased to 0.44 N s m^{-1}. Errors for wave speed and decay rate are expressed as relative error, while error for source angle is given as absolute error.

noise level				source angle α		wave speed V		decay rate β	
			SNR[a]	estimate[b]	abs err[c]	estimate	rel err	estimate	rel err
A_p	mean	variance	(dB)	(deg)	(deg)	(ms^{-1})	(%)	(m^{-1})	(%)
0.002	0	1.33×10^{-6}	39–46	59.67–60.02 (59.83, 0.12)	0.33	9.89–10.00 (9.94, 0.04)	1.1	1.78–2.29 (1.95, 0.15)	14.5
0.004	0	5.33×10^{-6}	27–34	59.43–59.92 (59.71, 0.19)	0.57	9.90–10.04 (9.97, 0.04)	1.0	1.15–2.47 (1.60, 0.38)	42.5
0.006	0	1.2×10^{-5}	19–27	59.39–60.05 (59.75, 0.21)	0.61	9.87–10.07 (9.95, 0.07)	1.3	0.41–2.16 (1.72, 0.54)	79.5
0.008	0	2.13×10^{-5}	14–22	59.47–60.43 (59.76, 0.31)	0.53	9.82–10.02 (9.92, 0.07)	1.8	0.37–3.44 (1.93, 1.00)	72.0
0.010	0	3.33×10^{-5}	11–18	59.12–60.50 (59.83, 0.43)	0.88	9.77–10.17 (9.97, 0.13)	2.3	1.09–3.61 (2.28, 0.88)	80.5

[a]It is the range of SNR for eight leg velocity responses.

[b]The estimation results are the ranges, the means (first parameter in the bracket) and standard deviations (second parameter in the bracket) of the estimated parameters in 10 runs.

[c]The error is the maximum error in 10 runs.

royalsocietypublishing.org/journal/rspa *Proc. R. Soc. A* **482**: 20250678

hard for the spiders to localize using the amplitude difference. Again, however, the decay rate is dependent on substrate choice and is less well studied for ecologically relevant substrates. Broadly speaking, decay rates of more flexible and freely vibrating substrates like plant stems and spider webs will be lower than stiffer soil/sand or rock-based ground substrates.

Our analyses also suggest distance-dependent constraints acting on source localization: that the spider may only be capable of estimating the source distance when the distance between spider and source is very close (about 1.25 times the leg span in this paper). Furthermore, the high decay rate of ground-based substrates in the natural environment, combined with the low amplitude of prey-generated vibrations, limits the distance over which biologically relevant vibrations propagate, possibly to the centimetre scale, depending on noise. We suggest that this is tolerable for the spider in its natural context. Tarantulas are sit-and-wait predators where moving in the right direction quickly might be sufficient for a successful ambush, where knowing distance to prey vibration sources might not be important to achieve prey capture. Triggering of a predatory response when the prey is more body lengths away from the spider may not be desirable as the ambush will take longer, so prey is more likely to escape and the spider will waste energy. For orb weaving spiders, it has also been suggested that knowing distance to the vibration source is not necessary for successful prey capture [45]. Although other cues may come into play for spider predatory behaviour, in our model animal *Grammostola pulchra*, vision is poorly developed and chemical sensing is likely to be too slow to aid in distance estimation. Hence, the most important parameter for the spider is likely to be vibration source angle, and not distance.

The analyses in §3f show that leg combinations that include the front and back two legs are the minimum leg requirement for source localization. Theoretically speaking, it is because these two pairs of legs are most distant from each other, so the time difference is maximized. Biologically speaking, these two pairs of legs are strategically positioned on spiders' bodies to maximize their exposure to vibrations across a planar surface. These legs are often extended forward and backward in a stereotypical posture, allowing spiders to pick up subtle changes in vibrations [47]. This is consistent with what is known from studies of spider orientation responses [8].

These results also indicate that our localization algorithm inspired by spiders is robust to noise and body damage. There are various circumstances where the spider vibration sensing can be affected by noise disturbances, e.g. external vibration from nearby machinery, vibration due to spider's own movement, and wind-induced vibration [34]. The results support that the spider may still be able to estimate the source angle accurately even if noise is relatively high, which needs further study. In terms of body damage, leg autotomy is a common occurrence in many spiders, and typically happens during moulting or in response to predator attack [48]. Some species also have the ability to regenerate lost legs over successive moults [49]. Our analyses show that the spider can still theoretically calculate source angle to a high degree of accuracy if some legs except the front and back pairs of legs are lost (table 7 and electronic supplementary material, table S1), which is commonly observed in wild spiders.

In theory, the leg stiffness and damping can be actively controlled by the spider via muscle action and/or hydrostatic pressure [50,51]. The analyses in §3g imply that the spiders may be able to improve the localization accuracy by increasing the leg–substrate contact damping.

Overall, these interpretations are intended to bridge our bio-inspired method and simulations with biological hypotheses. Further biological experiments with spiders will be needed to test these proposed biological implications. For example, behavioural studies with different spider species should aim to unpick the relative influences of noise, body morphology and posture (e.g. leg loss), substrate properties (i.e. decay rate, wave speed, dispersion) and sensor tuning (frequency-dependent sensory thresholds) on the predatory response behaviour.

(b) Advantage and disadvantage of the algorithm and configuration

Direct comparison among different vibration and impact localization studies is inherently difficult because the reported results can vary widely according to experimental setup, substrate, boundary conditions, sensor configuration, excitation type, assumptions, noise level, etc. Table 9

Table 9. The comparison with other representative studies/methods.

method	example reference	example environment and sensors	localization error	limitations
model + backward filter forward smoother + optimization based on time and amplitude differences	this work	simulation; 8 sensors	<3 deg for source angle	lose information of source distance
matched filter + TDOA	footstep localization [20]	real building; 12 accelerometers	RMSE = 0.59 m (in 25.5 m × 9.39 m hall); 0.81 m (in 15.79 m × 17.23 m lobby)	dense fixed array; need footstep templates
region localization method (sign of TDOA)	footstep localization [4]	indoor room; 9 sensors	0.29–0.68 m (in 3.6 m × 5.4 m room)	limited spatial accuracy
energy decay method	impact localization [21]	concrete corridor; 4 accelerometers	mean error = 0.25 m (in 2 m × 4 m corridor)	less robust to noise
model + Smoother filter + Newton Raphson optimization	impact identification [2]	composite panel; 12 piezoelectric sensors	average error = 24 mm max (in 0.61 m × 0.58 m panel)	need model
neural network + Wavelet transform	impact identification [14]	aluminium and composite plates; four piezoelectric sensors	max error = 2.96 mm (in 0.33 m × 0.33 m aluminium); 5.04 mm (in 0.33 m × 0.33 m composite)	need large training set
time-reversal method	vibration source localization [22]	Mower body frame; two piezoelectric patches	focusing spot diameter = half wavelength (about 2 cm in the 6 cm × 18 cm region)	require low propagation attenuation; limited spatial resolution

lists the comparison with some representative methods. Although this study is simulation-based, the achieved angle accuracy (less than 3 deg) up to a source distance of 10 m corresponds to a normalized spatial error on the order of 5%, better than the performance reported in large-scale experimental studies [4,20,21]. Unlike neural network methods [14], the proposed approach does not rely on extensive training data. Unlike the time-reversal method [22], it remains applicable to damped substrates. Unlike the energy decay method [21], it is more robust to noise.

The advantage of the algorithm is that it is applicable to any vibration source signal, rather than only applicable to certain types of signals, e.g. pulse in [52]. Rather than using spatially separated sensors attached on the substrate for vibration source localization, we propose that the sensors for vibration sensing are embedded and integrated into a spider-like prototype system. This configuration is more compact, convenient for signal synchronization and fusion, advantageous for movable applications (e.g. integrated into multi-legged robots [53]), and allows for real-time implementation of the algorithm and feedback. This configuration may potentially lead to a movable device capable of real-time localization and tracking of vibration sources. The drawback of this configuration is that it is not possible to estimate the source distance using one prototype, and it is difficult to localize the vibration source under high wave speeds unless the distance between the sensors is larger. However, the distance information may not be necessary in some scenarios, e.g. obstacle avoidance in robotics, where the robot only needs to turn away from the source to avoid collisions, search and rescue where rescuers only need to move towards the vibration source until they make direct contact, and security intrusion detection where guards only need to know the direction of the intrusion for investigation.

To allow for real-time tracking and localization of the vibration source, the running time of the localization algorithm should be short, which is dependent on many factors, e.g. number of sensors, sampling frequency, signal duration, optimization algorithm, etc. These factors will be considered to reduce the running time in real applications, but have not been considered in this paper.

The consideration of solely out-of-plane wave is based on the fact that the out-of-plane component constitutes most of the generated wave's energy compared to the in-plane components in some applications, e.g. in plates [54]. This is also based on the consideration that the out-of-plane waves monitoring is usually easier to be implemented and more robust to noise compared to in-plane waves in most applications.

The limitations of the algorithm are: (i) It is only applicable to non-dispersive waves, i.e. wave speed independent of frequency. This is a simplistic assumption, but it can still be reasonable for substrates or frequency ranges where dispersion is weak and the wave speed remains approximately constant. However, most real substrates exhibit some degree of dispersion, e.g. the floor in an indoor environment [4]. The dispersive property can distort the wave shape as the wave travels away from the vibration source [55], which can make the localization algorithm less effective. (ii) It is only applicable to substrates with constant decay rate. Constant decay rate is a reasonable assumption when the decay rate does not change significantly with the frequency [21], however, the decay rate may change significantly with the frequency in some cases. (iii) It is only applicable to the case with one vibration source. However, there can be multiple vibration sources in some situations. (iv) The limitation of the configuration itself, e.g. being unable to estimate the source distance, as discussed above.

According to the previous analyses, there are some suggestions that can be considered to improve the accuracy of localization in real application. Firstly, to use in substrates with high wave speeds, the distance between the sensors can be increased by increasing the leg span. Secondly, it is suggested to symmetrically embed sensors on six or eight legs which include the front and back two legs.

(c) Estimation of source distance

From the previous analyses, the algorithm based on one spider-like model cannot be used to estimate the vibration source distance when the source distance is much greater than the leg

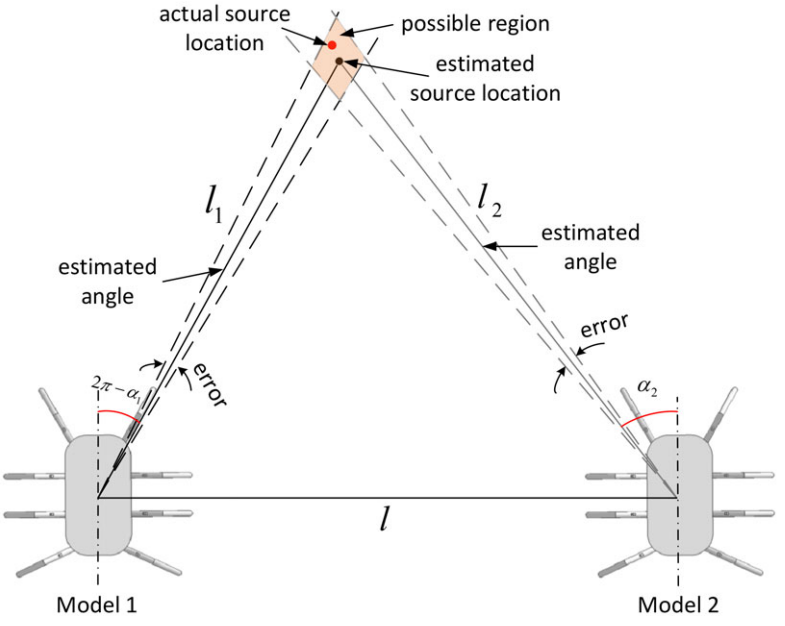

Figure 7. Diagram of generic engineering application to localize vibration source.

span, but the estimation of the source angle is accurate. In a real engineering application for localizing a vibration source, we suggest that two spatially separated spider-like models can be used concurrently. It is assumed that the actual source is not on the line connecting two models. Both models give an estimation of the source angle, so the estimated source location is at the intersection of these two directions, as shown in figure 7. The estimated source angles for model 1 and model 2 are α_1 and α_2, respectively. The distance between model 1 and model 2 is l. The estimated distances from model 1 and model 2 to the vibration source are l_1 and l_2, respectively.

The relationships are derived as follows:

$$\begin{cases} l_2^2 = l_1^2 + l^2 + 2l_1 l \sin\alpha_1, \\ l_1^2 = l_2^2 + l^2 - 2l_2 l \sin\alpha_2. \end{cases} \tag{4.1}$$

The estimated distances from model 1 and model 2 are solved from equation (4.1) as follows:

$$\begin{cases} l_1 = \frac{-l\cos\alpha_2}{\sin(\alpha_1-\alpha_2)}, \\ l_2 = \frac{-l\cos\alpha_1}{\sin(\alpha_1-\alpha_2)}. \end{cases} \tag{4.2}$$

Using two spider-like models, the source distance can be successfully estimated. Considering the error of the algorithm in estimating the source angles, there is a difference between the estimated source location and the actual source location. The error of the source angle estimation is dependent on many factors, e.g. noise, source distance, decay rate, wave speed. In real applications, it is also dependent on the modelling accuracy of the spider-like prototype. However, it gives a possible region where the actual source is located, as shown in figure 7.

5. Conclusion

The motivation of this paper is to develop technologies and algorithms that can be applied in engineering and understand how spiders may localize vibration sources. To this end, we develop a bio-inspired vibration source localization configuration and algorithm. The effectiveness of the algorithm is validated through simulations. The following conclusions can be drawn:

1. The localization algorithm gives accurate estimation of the source angle and wave speed with varying source distance, source angle, wave speed and decay rate, whose errors are usually within 3 deg (absolute) and 6% (relative), respectively. The estimation of the decay rate is less accurate.
2. The localization algorithm can only estimate the close source distance (less than 1.25 leg span), but it cannot estimate the distance when the distance becomes large (above 1.25 leg span) because both the time difference and amplitude ratio converge when the distance becomes large. Therefore, to locate the vibration source in a real engineering context, we suggest two spatially separated spider-like models used concurrently.
3. The localization algorithm is robust to leg responses with low signal-to-noise ratio.
4. By comparing different leg numbers and combinations, it is shown that the four-leg combination (including front and back two legs) is the minimum leg requirement for localization using the spider-like configuration, and adding legs to this basis would more or less increase the accuracy of the source angle prediction but at the expense of more equipment and increasing the computational cost. Any combinations without the consideration of the front and back two legs will not give satisfactory estimations. Increasing the leg-substrate contact damping would reduce the noise in the calculated leg inputs, thus improving the accuracy of the localization algorithm.

The results presented help us understand the mechanism and give us new insights into how spiders may localize the vibration source, particularly robustness of the system and distance-dependent constraints. Future research will be focused on the case of algorithm development for use in dispersive substrates and multiple vibration sources, prototype design and experimental validation.

Data accessibility. The data are provided in the electronic supplementary material [56].

Declaration of AI use. We have not used AI-assisted technologies in creating this article.

Authors' contributions. J.W.: conceptualization, formal analysis, investigation, methodology, software, validation, visualization, writing—original draft, writing—review and editing; T.E.M.: conceptualization, software, visualization, writing—review and editing; A.C.: investigation, writing—review and editing; G.T.: methodology, resources, supervision, writing—review and editing; B.M.: conceptualization, funding acquisition, methodology, project administration, resources, supervision, visualization, writing—review and editing.

All authors gave final approval for publication and agreed to be held accountable for the work performed therein.

Conflict of interest declaration. We declare we have no competing interests.

Funding. This work was supported by the Royal Society University Research Fellowship (grant no. URF\R1\191033).

References

1. Asgari S, Stafsudd JZ, Hudson RE, Yao K, Taciroglu E. 2015 Moving source localization using seismic signal processing. *J. Sound Vib.* **335**, 384–396. (doi:10.1016/j.jsv.2014.09.027)
2. Seydel R, Chang F-K. 2001 Impact identification of stiffened composite panels: I. System development. *Smart Mater. Struct.* **10**, 354. (doi:10.1088/0964-1726/10/2/323)
3. Choi K, Chang F-K. 1994 Identification of foreign object impact in structures using distributed sensors. *J. Intell. Mater. Syst. Struct.* **5**, 864–869. (doi:10.1177/1045389X9400500620)
4. Bahroun R, Michel O, Frassati F, Carmona M, Lacoume JL. 2014 New algorithm for footstep localization using seismic sensors in an indoor environment. *J. Sound. Vib.* **333**, 1046–1066. (doi:10.1016/j.jsv.2013.10.004)
5. Lee H, Park JW, Helal A. 2009 Estimation of indoor physical activity level based on footstep vibration signal measured by MEMS accelerometer in smart home environments. In *Mobile entity localization and tracking in GPS-less environnments: second international workshop* (eds R Fuller, XD Koutsoukos), pp. 148–162. Orlando, USA: Springer Berlin Heidelberg.
6. Hill PS. 2009 How do animals use substrate-borne vibrations as an information source? *Naturwissenschaften* **96**, 1355–1371. (doi:10.1007/s00114-009-0588-8)

7. Mortimer B. 2017 Biotremology: do physical constraints limit the propagation of vibrational information? *Anim. Behav.* **130**, 165–174. (doi:10.1016/j.anbehav.2017.06.015)
8. Hergenröder R, Barth FG. 1983 Vibratory signals and spider behavior: how do the sensory inputs from the eight legs interact in orientation? *J. Comp. Physiol.* **152**, 361–371. (doi:10.1007/BF00606241)
9. Miller TE, Mortimer B. 2020 Control vs. constraint: understanding the mechanisms of vibration transmission during material-bound information transfer. *Front. Ecol. Evol.* **8**, 587846. (doi:10.3389/fevo.2020.587846)
10. Barth FG. 2019 Mechanics to pre-process information for the fine tuning of mechanoreceptors. *J. Comp. Physiol. A Neuroethol. Sens. Neural Behav. Physiol.* **205**, 661–686. (doi:10.1007/s00359-019-01355-z)
11. Choi K, Chang F-K. 1996 Identification of impact force and location using distributed sensors. *AIAA J.* **34**, 136–142. (doi:10.2514/3.13033)
12. Tracy M, Chang F-K. 1998 Identifying impacts in composite plates with piezoelectric strain sensors, part I: theory. *J. Intell. Mater. Syst. Struct.* **9**, 920–928. (doi:10.1177/1045389X9800901108)
13. Jones RT, Sirkis JS, Friebele EJ. 1997 Detection of impact location and magnitude for isotropic plates using neural networks. *J. Intell. Mater. Syst. Struct.* **8**, 90–99. (doi:10.1177/1045389X9700800109)
14. Sung D-U, Oh J-H, Kim C-G, Hong C-S. 2000 Impact monitoring of smart composite laminates using neural network and wavelet analysis. *J. Intell. Mater. Syst. Struct.* **11**, 180–190. (doi:10.1106/n5e7-m37y-3mar-2kfh)
15. Adams R, Doyle JF. 2002 Multiple force identification for complex structures. *Exp. Mech.* **42**, 25–36. (doi:10.1007/BF02411048)
16. Trujillo DM. 1978 Application of dynamic programming to the general inverse problem. *Int. J. Numer. Methods Eng.* **12**, 613–624. (doi:10.1002/nme.1620120406)
17. Busby HR, Trujillo DM. 1987 Solution of an inverse dynamics problem using an eigenvalue reduction technique. *Comput. Struct.* **2**, 109–117. (doi:10.1016/0045-7949(87)90222-7)
18. Inoue H, Harrigan JJ, Reid SR. 2001 Review of inverse analysis for indirect measurement of impact force. *Appl. Mech. Rev.* **54**, 503–524. (doi:10.1115/1.1420194)
19. Pezerat CJ, Guyader L. 2000 Identification of vibration sources. *Appl. Acoust.* **61**, 309–324. (doi:10.1016/S0003-682X(00)00036-0)
20. Poston JD, Buehrer RM, Tarazaga PA. 2017 Indoor footstep localization from structural dynamics instrumentation. *Mech. Syst. Signal Process.* **88**, 224–239. (doi:10.1016/j.ymssp.2016.11.023)
21. Alajlouni SE, Albakri M, Tarazaga P. 2018 Impact localization in dispersive waveguides based on energy-attenuation of waves with the traveled distance. *Mech. Syst. Signal Process.* **105**, 361–376. (doi:10.1016/j.ymssp.2017.12.007)
22. Vigoureux D, Guyader J-L. 2012 A simplified time reversal method used to localize vibrations sources in a complex structure. *Appl. Acoust.* **73**, 491–496. (doi:10.1016/j.apacoust.2011.12.004)
23. Barth FG. 2008 Cupiennius (Araneae, Ctenidae): biology and sensory ecology of a model spider. *Stapfia* **88**, 211–224.
24. Barth FG, Geethabali. 1982 Spider vibration receptors: threshold curves of individual slits in the metatarsal lyriform organ. *J. Comp. Physiol* **148**, 175–185. (doi:10.1007/BF00619124)
25. Landolfa MA, Barth FG. 1996 Vibrations in the orb web of the spider Nephila clavipes: cues for discrimination and orientation. *J. Comp. Physiol. A* **179**, 493–508. (doi:10.1007/BF00192316)
26. Seyfarth EA, Hergenröder R, Ebbes H, Barth FG. 1982 Idiothetic orientation of a wandering spider: compensation of detours and estimates of goal distance. *Behav. Ecol. Sociobiol.* **11**, 139–148. (doi:10.1007/BF00300103)
27. Čokl A, Virant-Doberlet M, McDowell A. 1999 Vibrational directionality in the southern green stink bug, Nezara viridula (L.), is mediated by female song. *Anim. Behav.* **58**, 1277–1283. (doi:10.1006/anbe.1999.1272)
28. Goulson D, Birch MC, Wyatt TD. 1994 Mate location in the deathwatch beetle, Xestobium rufovillosum De Geer (Anobiidae): orientation to substrate vibrations. *Anim. Behav.* **47**, 899–907. (doi:10.1006/anbe.1994.1122)
29. Masters WM, Markl H. 1981 Vibration signal transmission in spider orb webs. *Science* **213**, 363–365. (doi:10.1126/science.213.4505.363)

30. Elias DO, Mason AC, Hoy RR. 2004 The effect of substrate on the efficacy of seismic courtship signal transmission in the jumping spider Habronattus dossenus (Araneae: Salticidae). *J. Exp. Biol.* **207**, 4105–4110. (doi:10.1242/jeb.01261)
31. Virant-Doberlet M, Cokl A. 2004 Vibrational communication in insects. *Neotrop. Entomol.* **33**, 121–134. (doi:10.1590/S1519-566X2004000200001)
32. Mortimer B, Soler A, Siviour CR, Vollrath F. 2018 Remote monitoring of vibrational information in spider webs. *Naturwissenschaften* **105**, 37. (doi:10.1007/s00114-018-1561-1)
33. Bosia F *et al.* 2022 Optimized structures for vibration attenuation and sound control in nature: a review. *Matter* **5**, 3311–3340. (doi:10.1016/j.matt.2022.07.023)
34. Wu C-H, Elias DO. 2014 Vibratory noise in anthropogenic habitats and its effect on prey detection in a web-building spider. *Anim. Behav.* **90**, 47–56. (doi:10.1016/j.anbehav.2014.01.006)
35. Bleckmann H, Barth FG. 1984 Sensory ecology of a semi-aquatic spider (*Dolomedes triton*) II. The release of predatory behavior by water surface waves. *Behav. Ecol. Sociobiol.* **14**, 303–312. (doi:10.1007/BF00299502)
36. Vollrath F. 1987 Altered geometry of webs in spiders with regenerated legs. *Nature* **328**, 247–248. (doi:10.1038/328247a0)
37. Fraser C, Wede J, Uetz GW. 2020 Limb autotomy and regeneration affect vibratory/seismic courtship signaling and female receptivity in wolf spiders. *J. Arachnol.* **48**, 132–139. (doi:10.1636/0161-8202-48.2.132)
38. Lott M, Poggetto VFD, Greco G, Pugno NM, Bosia F. 2022 Prey localization in spider orb webs using modal vibration analysis. *Sci. Rep.* **12**, 19045. (doi:10.1038/s41598-022-22898-3)
39. Dal Poggetto VF, Bosia F, Greco G, Pugno NM. 2022 Prey impact localization enabled by material and structural interaction in spider orb webs. *Adv. Theory Simul.* **5**, 2100282. (doi:10.1002/adts.202100282)
40. Otto AW, Elias DO, Hatton RL. 2018 Modeling transverse vibration in spider webs using frequency-based dynamic substructuring. In *Proc. 36th IMAC, Conf. on Exposition on Structural Dynamics*. Springer Cham, Switzerland: International Publishing.
41. Naderinejad M, Junge K, Hughes J. 2023 Exploration of the design of spiderweb-inspired structures for vibration-driven sensing. *Biomimetics (Basel)* **8**, 111. (doi:10.3390/biomimetics8010111)
42. Zhao XF *et al.* 2021 Spider web-like flexible tactile sensor for pressure-strain simultaneous detection. *ACS Appl. Mater. Interfaces* **13**, 10 428–10 436. (doi:10.1021/acsami.0c21960)
43. Wu J, Miller TE, Cicirello A, Mortimer B. 2023 Spider dynamics under vertical vibration and its implications for biological vibration sensing. *J. R. Soc. Interface* **20**, 20230365. (doi:10.1098/rsif.2023.0365)
44. Wu J, Qiu Y. 2020 Modelling of seated human body exposed to vertical, lateral and roll vibration. *J. Sound Vib.* **485**, 115509. (doi:10.1016/j.jsv.2020.115509)
45. Mortimer B, Soler A, Wilkins L, Vollrath F. 2019 Decoding the locational information in the orb web vibrations of Araneus diadematus and Zygiella x-notata. *J. R. Soc. Interface* **16**, 20190201. (doi:10.1098/rsif.2019.0201)
46. Hergenröder R, Barth FG. 1983 The release of attack and escape behavior by vibratory stimuli in a wandering spider (Cupiennim salei) keys. *J. Comp. Physiol.* **152**, 347–359. (doi:10.1007/BF00606240)
47. Klärner D, Barth FG. 1982 Vibratory signals and prey capture in orb-weaving spiders (Zygiella x-notata, Nephila clavipes; Araneidae). *J. Comp. Physiol.* **148**, 445–455. (doi:10.1007/BF00619783)
48. Brown CA, Amaya CC, Formanowicz Jr DR. 2018 The frequency of leg autotomy and its influence on survival in natural populations of the wolf spider Pardosa valens. *Can. J. Zool.* **96**, 973–979. (doi:10.1139/cjz-2017-0262)
49. Vollrath F. 1995 Lyriform organs on regenerated spider legs. *Bull. Br. Arachnol. Soc.* **10**, 115–118.
50. Wilson RS. 1970 Some comments on the hydrostatic system of spiders (Chelicerata, Araneae). *Z. Morph. Tiere* **68**, 308–322. (doi:10.1007/BF00376004)
51. Blickhan R. 1986 Stiffness of an arthropod leg joint. *J. Biomech.* **19**, 375–384. (doi:10.1016/0021-9290(86)90014-X)
52. Yan G, Zhou L. 2009 Impact load identification of composite structure using genetic algorithms. *J. Sound Vib.* **319**, 869–884. (doi:10.1016/j.jsv.2008.06.051)
53. Saranli U, Buehler M, Koditschek DE. 2001 RHex: a simple and highly mobile hexapod robot. *Int. J. Rob. Res.* **20**, 616–631. (doi:10.1177/02783640122067570)

54. Ziola SM. 1991 *Source location in thin plates using cross-correlation*. Monterey, CA: Naval Postgraduate School.
55. De Marchi L, Marzani A, Speciale N, Viola E. 2011 A passive monitoring technique based on dispersion compensation to locate impacts in plate-like structures. *Smart Mater. Struct.* **20**, 035021. (doi:10.1088/0964-1726/20/3/035021)
56. Wu J, Miller TE, Cicirello A, Taylor G, Mortimer B. 2026 A bio-inspired configuration and algorithm for vibration source localization and its biological implications. Fighsare. (doi:10.6084/m9.figshare.c.8297065)